



ELSEVIER

Physica A 280 (2000) 315–336

PHYSICA A

www.elsevier.com/locate/physa

Period stabilization in the Busse–Heikes model of the Küppers–Lortz instability

R. Toral*, M. San Miguel, R. Gallego

Department de Física, Institut Mediterràneo de Estudios Avanzados (UIB-CSIC), Universitat de Les Illes Balears E-07071 Palma de Mallorca, Spain¹

Received 18 January 2000

Abstract

The Busse–Heikes dynamical model is described in terms of relaxational and non-relaxational dynamics. Within this dynamical picture a diverging alternating period is calculated in a reduced dynamics given by a time-dependent Hamiltonian with decreasing energy. A mean period is calculated which results from noise stabilization of a mean energy. The consideration of spatial-dependent amplitudes leads to vertex formation. The competition of front motion around the vertices and the Küppers–Lortz instability in determining an alternating period is discussed. © 2000 Elsevier Science B.V. All rights reserved.

Keywords: Küppers–Lortz instability in rotating convection; Front motion; Non-potential effects; Noise in heteroclinic orbits

Dedicated to Joel Lebowitz on the occasion of his 70th birthday

1. Introduction

One of the most extensively studied systems, in the field of pattern formation in non-equilibrium systems, is Rayleigh–Bénard thermal convection. In many geophysical and astrophysical systems, thermally induced convection is combined with Coriolis forces induced by rotation. Therefore, Rayleigh–Bénard convection in fluid layers rotating around a vertical axis is a hydrodynamical system of significant importance. Specially interesting is a spatio-temporal regime that takes place above a critical rotation angular velocity. The system breaks up into a persistent dynamical state such that set of parallel convection rolls are seen to change orientation with a characteristic

* Corresponding author. Fax: +34-971 173 426.

E-mail address: raul@imedea.uib.es (R. Toral)

¹ Web site: <http://www.imedea.uib.es/PhysDept/>

period. This phenomenon is known as the Küppers–Lortz instability [1]. This instability can be described as follows: for an angular rotation speed Ω greater than some critical value Ω_c , convective rolls lose their stability with respect to rolls inclined at an angle of about 60° in the sense of rotation. The new rolls undergo the same instability, so that there is no stable steady-state pattern. As a result spatially disordered patterns arise already arbitrarily close to the onset of convection. Experimental characterization of this regime of spatio-temporal chaos has been reported in [2,3]. Most experiments have been performed for small Prandtl numbers and have been theoretically described in the realm of Swift–Hohenberg models with [4,5] and without [6–8] the inclusion of mean flow effects. On the other hand, large Prandtl numbers lead to more rigid convection rolls. In this situation mean flow coupling can be neglected and, in the limit of infinite Prandtl numbers, three-mode models have been shown [9,10] to exhibit the same qualitative features as more sophisticated Swift–Hohenberg models that take into account the full range of possible roll orientations.

We consider in this paper a three-mode model proposed by Busse and Heikes [11] to study the Küppers–Lortz instability. Each mode represents the amplitude of a set of parallel rolls with an orientation of 60° to each other. This model contains an attracting heteroclinic cycle connecting three fixed points corresponding to the three different roll solutions. The model predicts successfully the existence of a region in parameter space in which the roll solution is unstable, but fails to reproduce the experimental observation of an approximately constant period between roll alternation. Whereas Busse and Heikes speculated that such a constant period would be obtained by the addition of noise, a conclusion confirmed by Stone and Holmes [12], no systematic study of the relation of the period to the system parameters has been performed so far. Another explanation for period stabilization has been given by Cross and Tu [9], who have performed numerical investigations of an extension of the Busse–Heikes equations, where a spatial variation of the amplitudes has been introduced. In this paper, we study in detail these two proposed mechanisms for period stabilization in the Busse–Heikes model: (i) addition of noise and (ii) the consideration of spatial-dependent terms.

The paper is organized as follows. In Section 2 we present a description of the Busse–Heikes model and give a clear physical explanation of the period divergence. We describe the dynamics in terms of a relaxational and a non-relaxational part. The alternating period is calculated for the latter part which is associated with a slowly varying time-dependent Hamiltonian. In Section 3 we consider the same model with the inclusion of additive white noise terms and we calculate the mean period stabilized by noise in terms of the previous dynamical picture. Sections 2 and 3 discuss ordinary differential equations for the amplitudes of the three modes. In Section 4 we consider the more physically appropriate situation of spatial-dependent amplitudes in a $d = 2$ model and study the influence on the dynamics of isotropic and anisotropic spatial-dependent terms. We describe the formation of vertices and how the period of roll alternation is determined by the competition of front motion around the vertices and the Küppers–Lortz instability.

2. Busse–Heikes model

Based on the fact that, in a first approximation, only three directions are relevant to this problem, Busse and Heikes [11] proposed a dynamical model to study the Küppers–Lortz instability. The vertical component of the velocity field $\Psi(\mathbf{r}, t)$ is written as

$$\Psi(\mathbf{r}, t) = \sum_{j=1}^3 A_j(\mathbf{r}, t) e^{iq_0 \hat{\mathbf{e}}_j \cdot \mathbf{r}} + \text{c.c.} \quad (1)$$

(“c.c.” denotes complex conjugate). The vectors $\hat{\mathbf{e}}_j$ are unit vectors in directions $j = 1, 2, 3$ which form an angle of 60° between them, and q_0 is the selected wave number of the convection pattern. In this model the (complex) amplitudes of the three rotating modes, A_1, A_2, A_3 , are independent of space and follow the evolution equations [11]:

$$\begin{aligned} \dot{A}_1 &= A_1[v - |A_1|^2 - (1 + \mu + \delta)|A_2|^2 - (1 + \mu - \delta)|A_3|^2], \\ \dot{A}_2 &= A_2[v - |A_2|^2 - (1 + \mu + \delta)|A_3|^2 - (1 + \mu - \delta)|A_1|^2], \\ \dot{A}_3 &= A_3[v - |A_3|^2 - (1 + \mu + \delta)|A_1|^2 - (1 + \mu - \delta)|A_2|^2]. \end{aligned} \quad (2)$$

The parameter v is proportional to the difference between the Rayleigh number and the the critical Rayleigh number for convection. We will consider exclusively in this paper the case of well-developed convection for which the parameter v can be rescaled to 1, i.e., $v = 1$ henceforth. The exact relation of μ and δ to the fluid properties has been given in [1]. We mention here that μ is a parameter related to the temperature gradient and the Taylor number (proportional to the rotation speed Ω) in such a way that it takes a non-zero value in the case of no rotation, $\Omega = 0$, whereas δ is related to the Taylor number in such a way that $\Omega = 0$ implies $\delta = 0$. We will consider only $\Omega > 0$, or $\delta > 0$; the case $\Omega < 0$ ($\delta < 0$) follows by a simple change of the coordinate system. Although the dynamical equations are defined for all values of the parameters, only the case $\mu \geq 0$ is physically relevant. Writing $A_j = \sqrt{R_j} e^{i\theta_j}$ we obtain equations for the modulus square of the amplitudes R_j :

$$\begin{aligned} \dot{R}_1 &= 2R_1[1 - R_1 - (1 + \mu + \delta)R_2 - (1 + \mu - \delta)R_3], \\ \dot{R}_2 &= 2R_2[1 - R_2 - (1 + \mu + \delta)R_3 - (1 + \mu - \delta)R_1], \\ \dot{R}_3 &= 2R_3[1 - R_3 - (1 + \mu + \delta)R_1 - (1 + \mu - \delta)R_2] \end{aligned} \quad (3)$$

and for the phases θ_j :

$$\begin{aligned} \dot{\theta}_1 &= 0, \\ \dot{\theta}_2 &= 0, \\ \dot{\theta}_3 &= 0. \end{aligned} \quad (4)$$

It follows that the phases are simply arbitrary constants fixing the location of the rolls. A solution of the form $\Psi(\mathbf{r}) = \sqrt{R_j} e^{i(q_0 \hat{\mathbf{e}}_j \cdot \mathbf{r} + \theta_j)} + \text{c.c.}$ represents a set of rolls of

wavelength $2\pi/q_0$, oriented in a direction perpendicular to the vector \hat{e}_j . Hence, in this model one can simply consider the equations for the real variables R_j instead of the equations for the complex variables A_j . A similar set of equations has been proposed to study population competition dynamics. For a single biological species, the Verhulst or logistic model assumes that its population $N(t)$ satisfies the evolution equation:

$$\frac{dN}{dt} = rN(1 - \lambda N), \quad (5)$$

where r is the reproductive growth rate and λ is a coefficient denoting competition amongst the members of the species. If three species are competing together, it is adequate in some occasions to model this competition by introducing a Gause–Lotka–Volterra type of equations [13,14]:

$$\begin{aligned} \dot{N}_1 &= rN_1(1 - \lambda N_1 - \alpha N_2 - \beta N_3), \\ \dot{N}_2 &= rN_2(1 - \lambda N_2 - \alpha N_3 - \beta N_1), \\ \dot{N}_3 &= rN_3(1 - \lambda N_3 - \alpha N_1 - \beta N_2), \end{aligned} \quad (6)$$

which are the same that the Busse–Heikes equations (3) for the modulus square of the amplitudes R_j with the identifications: $r=2$, $\lambda=1$, $\alpha=1+\mu+\delta$, $\beta=1+\mu-\delta$. These equations are the basis of May and Leonard analysis [13]. We also mention the work of Soward [15] which is concerned with the study of the nature of the bifurcations mainly, but not limited to, close to the convective instability for small v , in a slightly more general model that includes also quadratic non-linearities in the equations. In the remaining of the section we will analyze some of the properties of the solutions of the Busse–Heikes equations (2). Although our analysis essentially reobtains the results of May and Leonard, we find it convenient to give it in some detail because, besides obtaining some further analytical expressions for the time variation of the amplitudes, we are able in some cases of rewriting the dynamics in terms of a Lyapunov potential. The existence of this Lyapunov potential allows us to interpret the asymptotic dynamics for $\mu=0$ as a residual (conservative) Hamiltonian dynamics. For $\mu>0$ we will use an adiabatic approximation with a time-dependent Hamiltonian. This interpretation will turn out to be very useful in the case that noise terms are added to the dynamical equations, because the found Lyapunov potential governs approximately the stationary probability distribution.

We first look for stationary solutions of the Busse–Heikes equations (2). The fixed point solutions are the following:

(a) The *null* solution: $R_1 = R_2 = R_3 = 0$.

(b) *Roll* solutions. There are three families of these solutions, each characterized by a unique nonvanishing amplitude, for instance: $(R_1, R_2, R_3) = (1, 0, 0)$ is a roll solution with rolls perpendicular to the \hat{e}_1 direction, and so on.

(c) *Hexagon* solutions. The three amplitudes are equal and different from 0, namely $R_1 = R_2 = R_3 = 1/(3+2\mu)$. They only exist for $\mu > -\frac{3}{2}$.

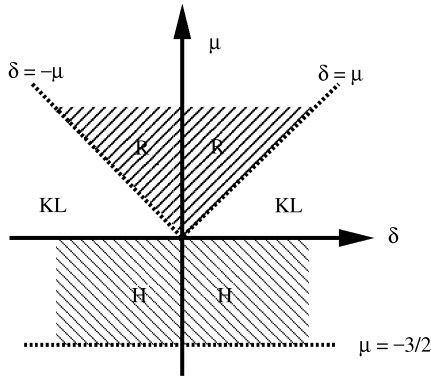


Fig. 1. Stability regions for the Busse–Heikes dynamical system (2). The region ‘H’ is where the hexagon solution (three equal amplitudes) is stable. In the ‘R’ region, the three roll solutions are stable, and in region ‘KL’ there are no stable fixed points.

(d) *Rhombus* solutions. There are three families of these solutions, in which two amplitudes are different from 0 and the third amplitude vanishes. For instance: $(R_1, R_2, R_3) = ((\mu + \delta)/[\mu(\mu + 2) - \delta^2], (\mu - \delta)/[\mu(\mu + 2) - \delta^2], 0)$. They only exist for $\mu > \delta$, or $-1 - \sqrt{1 + \delta^2} < \mu < -\delta$.

The stability of the previous solutions can be studied by means of a linear stability analysis. The result is summarized in Fig. 1. For $\mu < -\frac{3}{2}$ there are no stable solutions and the amplitudes grow without limit. The rhombus and null solutions are never stable. The hexagon solutions are stable for $-\frac{3}{2} < \mu < 0$. The roll solutions are stable for $\mu > \delta$. For $0 < \mu < \delta$ there are no stable solutions, but the amplitudes remain bounded. This instability can be described as follows: consider the unstable roll solution $(R_1, R_2, R_3) = (1, 0, 0)$. The amplitude of the A_2 mode starts growing and that of A_1 decreasing in order to reach the roll solution $(0, 1, 0)$. However, this new roll solution is also unstable, and before it can be reached, the dynamical system starts evolving towards the roll solution $(0, 0, 1)$, which is unstable and evolves towards the solution $(1, 0, 0)$ which is unstable, and so on. Schematically, we can represent the situation as follows:

$$(1, 0, 0) \rightarrow (0, 1, 0) \rightarrow (0, 0, 1) \rightarrow (1, 0, 0) \rightarrow (0, 1, 0) \dots \quad (7)$$

This is the Küppers–Lortz instability that shows up in the rotation of the convective rolls. The Küppers–Lortz unstable region is characterized by the presence of three unstable fixed points, and a heteroclinic cycle connecting them.

The novelty of our treatment consists in writing the Busse–Heikes equations of motion in the form

$$\dot{A}_j = -\frac{\partial V}{\partial A_j^*} + \delta v_j, \quad j = 1, 2, 3, \quad (8)$$

with the *potential function*

$$\begin{aligned} V(A_1, A_2, A_3) &= -(|A_1|^2 + |A_2|^2 + |A_3|^2) + \frac{1}{2}(|A_1|^4 + |A_2|^4 + |A_3|^4) \\ &\quad + (1 + \mu)(|A_1|^2|A_2|^2 + |A_2|^2|A_3|^2 + |A_3|^2|A_1|^2) \\ &= -(R_1 + R_2 + R_3) + \frac{1}{2}(R_1^2 + R_2^2 + R_3^2) \\ &\quad + (1 + \mu)(R_1R_2 + R_2R_3 + R_3R_1) \end{aligned} \quad (9)$$

and

$$\begin{aligned} v_1 &= A_1(-|A_2|^2 + |A_3|^2) = A_1(-R_2 + R_3), \\ v_2 &= A_2(-|A_3|^2 + |A_1|^2) = A_2(-R_3 + R_1), \\ v_3 &= A_3(-|A_1|^2 + |A_2|^2) = A_3(-R_1 + R_2). \end{aligned} \quad (10)$$

The first term on the right-hand side of (8) describes relaxation in the potential $V(A_1, A_2, A_3)$. In the case $\delta = 0$, hence, the dynamics is described simply as the relaxation, along the gradient lines of the potential V , in order to reach a minimum of V . In the case $\delta > 0$ there is another contribution to the dynamics. Its effect can be analyzed partly by looking at the time evolution of the potential:

$$\frac{dV}{dt} = \sum_{j=1}^3 \frac{\partial V}{\partial A_j} \frac{dA_j}{dt} + \text{c.c.} = -2 \sum_{j=1}^3 \left| \frac{\partial V}{\partial A_j} \right|^2 + \delta \left[\sum_{j=1}^3 \frac{\partial V}{\partial A_j} v_j + \text{c.c.} \right]. \quad (11)$$

Therefore, when the so-called *orthogonality condition* is satisfied

$$\delta \left[\sum_{j=1}^3 \frac{\partial V}{\partial A_j} v_j + \text{c.c.} \right] = 0, \quad (12)$$

the function V decreases along the dynamical trajectories and it becomes a Lyapunov potential [16] if it is bounded from below (which is the case for $\mu > -3/2$). Using Eqs. (9) and (10), Eq. (11) can be rewritten as

$$\frac{dV}{dt} = -2 \sum_{j=1}^3 \left| \frac{\partial V}{\partial A_j} \right|^2 - 2\mu\delta(|A_1|^2 - |A_2|^2)(|A_2|^2 - |A_3|^2)(|A_3|^2 - |A_1|^2), \quad (13)$$

so that the orthogonality condition is seen to be satisfied for $\mu\delta = 0$. In the case $\delta = 0$, the system is purely relaxational in the potential V and the corresponding stability diagram can be obtained also by looking at the minima of V . For the null solution, the potential takes the value $V = 0$; for the rhombus, $V = -1/(2 + \mu)$; for the roll solution, $V = -\frac{1}{2}$; and, finally, for the hexagon solution, $V = -3/(6 + 4\mu)$. The study of the potential (for $\delta = 0$) shows that the null and rhombus solutions correspond always to maxima of the potential and are, therefore, unstable everywhere. It turns out that the rolls (hexagons) are maxima (minima) of the potential for $\mu < 0$ and minima (maxima) for $\mu > 0$. Also, the potential for the roll solution is smaller than the potential for the other solutions whenever $\mu > 0$, indicating that the rolls are the most stable

(and indeed the only stable ones) solutions in this case. Unfortunately, this simple criterion does not have an equivalent in the non-relaxational case, $\delta > 0$, for which one has to perform the full linear stability analysis.

2.1. *The case $\mu = 0$*

According to the result (13), the function $V(A_1, A_2, A_3)$ is a Lyapunov potential whenever $\mu\delta = 0$. As discussed in the previous section, the case $\delta = 0$ implies a relaxational gradient dynamics in which all variables tend to fixed values. In the case $\mu = 0, \delta > 0$, the dynamics is non-relaxational potential [17–19] and, whereas the dynamics still leads to the surface of minima of the Lyapunov function, there is a residual motion in this surface for which $dV/dt = 0$. In other words: the relaxational terms in the dynamics make the system evolve towards the degenerate minimum of the potential (which for $\mu=0$ occurs at $R_1 + R_2 + R_3 = 1$). The residual motion is governed by the non-relaxational part which is proportional to δ and this residual motion disappears for $\delta = 0$, the relaxational gradient case.

According to this reduction of the dynamics as a residual motion in the surface of minima of the potential V , strictly valid only for $\mu = 0$, it turns out that it is possible to solve essentially the equations of motion. By “essentially” we mean that after a transient time in which the system is driven to the minima of V , the residual motion is a conservative one in which it is possible to define a Hamiltonian-like function that allows one to find explicit expressions for the time variation of the dynamical variables. Let us define the variable

$$X(t) = R_1 + R_2 + R_3 . \tag{14}$$

It is straightforward to show that, for arbitrary μ and δ , X satisfies the evolution equation

$$\dot{X} = 2X(1 - X) - 4\mu Y , \tag{15}$$

where

$$Y(t) = R_1R_2 + R_2R_3 + R_3R_1 . \tag{16}$$

In the case $\mu = 0$ the equation for $X(t)$ is a closed equation whose solution is

$$X(t) = \frac{1}{(\frac{1}{X_0} - 1)e^{-2t} + 1} . \tag{17}$$

Here $X_0 = X(t=0)$. From this expression it turns out that $\lim_{t \rightarrow \infty} X(t) = 1$ independently of the initial condition. In practice, and due to the exponential decay towards 1 of the above expression, after a transient time of order 1, $X(t)$ already takes its asymptotic value $X(t) = 1$. Therefore, we can substitute $R_1(t)$, say, by $1 - R_2(t) - R_3(t)$ to obtain evolution equations for $R_2(t)$ and $R_3(t)$. In this way, the original 3-variable problem, Eqs. (3), is reduced to a residual dynamics in a 2-variable subspace:

$$\dot{R}_2 = 2\delta R_2(1 - R_2 - 2R_3) , \tag{18}$$

$$\dot{R}_3 = -2\delta R_3(1 - 2R_2 - R_3) . \tag{19}$$

These are Hamilton's equations

$$\dot{R}_2 = 2\delta \frac{\partial \mathcal{H}}{\partial R_3}, \quad (20)$$

$$\dot{R}_3 = -2\delta \frac{\partial \mathcal{H}}{\partial R_2}, \quad (21)$$

corresponding to the Hamiltonian

$$\mathcal{H}(R_2, R_3) = R_2 R_3 (1 - R_2 - R_3). \quad (22)$$

As a consequence, in the asymptotic dynamics for which the Hamiltonian description is valid, $\mathcal{H}(t)$ is a constant of motion, $\mathcal{H} = E$, which will be called the "energy". The Hamiltonian dynamics is valid only after a transient time, but the value of E depends only on initial conditions at $t = 0$. The dependence of E on the initial conditions can be found by introducing the variable $\hat{\mathcal{H}}$:

$$\hat{\mathcal{H}} = R_1 R_2 R_3, \quad (23)$$

which, in the asymptotic limit ($t \rightarrow \infty$) is equivalent to \mathcal{H} . It is easy to show that, for arbitrary values of μ and δ , $\hat{\mathcal{H}}$ satisfies the following evolution equation:

$$\hat{\mathcal{H}}^{-1} \frac{d\hat{\mathcal{H}}}{dt} = 6 - (6 + 4\mu)X \quad (24)$$

(one can reduce the original dynamical problem to variables $\{X, Y, \hat{\mathcal{H}}\}$ but the equation for \dot{Y} turns out to be too complicated, see [15]). If we substitute the solution for $X(t)$ valid in the case $\mu = 0$ we obtain

$$\hat{\mathcal{H}}(t) = \hat{\mathcal{H}}_0 [(1 - X_0)e^{-2t} + X_0]^{-3}, \quad (25)$$

with $\hat{\mathcal{H}}_0 = \hat{\mathcal{H}}(t = 0)$. The asymptotic value for \mathcal{H} is

$$E = \lim_{t \rightarrow \infty} \mathcal{H}(t) = \lim_{t \rightarrow \infty} \hat{\mathcal{H}}(t) = \frac{\hat{\mathcal{H}}_0}{X_0^3} = \frac{R_1(0)R_2(0)R_3(0)}{(R_1(0) + R_2(0) + R_3(0))^3}. \quad (26)$$

Again, this asymptotic value is reached after a transient time of order 1. This expression suggests to define the time-dependent variable

$$E(t) = \frac{\hat{\mathcal{H}}}{X^3} = \frac{R_1 R_2 R_3}{(R_1 + R_2 + R_3)^3}, \quad (27)$$

whose evolution equation (again, for arbitrary μ, δ) is

$$\frac{dE}{dt} = -4\mu \left(X - 3 \frac{Y}{X} \right) E \equiv -4\mu f(t)E. \quad (28)$$

Therefore, in the case $\mu = 0$, $E(t) = E$ is a constant of motion that coincides, in the asymptotic limit when $X = 1$, with the numerical value of the Hamiltonian \mathcal{H} . According to their definition, $E(t)$ is a bounded function $0 \leq E(t) \leq \frac{1}{27}$ and $f(t) \geq 0$ for $R_j \geq 0$, $j = 1, 2, 3$.

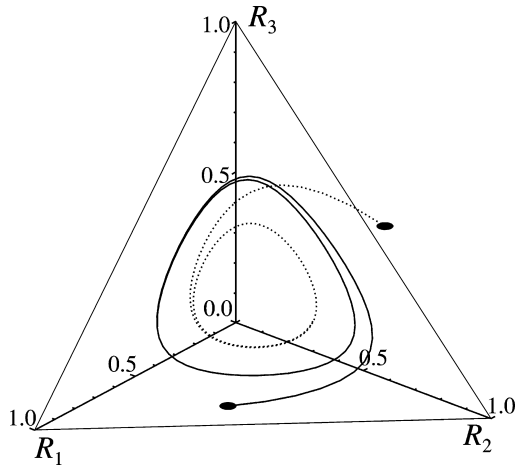


Fig. 2. Dynamics for $\mu = 0$ in the variables R_1, R_2, R_3 for two different initial conditions. After a transient time of order 1 the motion is on the plane $R_1 + R_2 + R_3 = 1$.

The problem in the case $\mu = 0$ can now be given an explicit solution. After a transient time (or order 1), the motion occurs on the plane $R_1 + R_2 + R_3 = 1$; see Fig. 2. The motion is periodic because it corresponds to a Hamiltonian orbit with a fixed energy. The exact shape of the trajectory depends on the value of the energy E which, in turn, depends on initial conditions. More interestingly, the period of the orbit can also be computed. For this, we solve the evolution equation (again asymptotically) for, say, R_3 . By the elimination of R_2 by setting $\mathcal{H} = E$ in Eq. (22)

$$R_2 = \frac{1}{2}(1 - R_3 \pm \sqrt{(1 - R_3)^2 - 4E/R_3}), \tag{29}$$

we obtain a closed equation for R_3

$$\dot{R}_3 = \pm 2\delta \sqrt{R_3^2(1 - R_3)^2 - 4ER_3}. \tag{30}$$

Let b and c be the return points, i.e., the solutions of

$$R_3(1 - R_3)^2 - 4E = 0, \tag{31}$$

lying in the interval $(0, 1)$.² The three roots, a, b, c , of the above third-degree equation are real and two of them (the return points b, c) lie in the interval $(0, 1)$. The explicit expression for the roots is

$$a = \frac{2}{3} \left[1 + \cos \frac{\theta}{3} \right], \tag{32}$$

$$b = \frac{2}{3} \left[1 + \cos \frac{\theta - 2\pi}{3} \right], \tag{33}$$

$$c = \frac{2}{3} \left[1 + \cos \frac{\theta + 2\pi}{3} \right], \tag{34}$$

² The case $R_3 = 0$ necessarily leads to $E = 0$ and the dynamics stops.

where

$$\theta = \arccos(54E - 1). \quad (35)$$

Integration of (30) yields the equation of motion for $R_3(t)$

$$\int_c^{R_3(t)} \frac{dx}{\sqrt{x(x-a)(x-b)(x-c)}} = 2\delta \int_{t_0}^t dt', \quad (36)$$

where we have chosen the initial time t_0 to correspond to the minimum value when $R_3(t) = c$. The integral on the left-hand side can be expressed in terms of the Jacobi elliptic function [20] $\operatorname{sn}[x|q]$, to yield

$$R_3(t) = \frac{bc}{b + (c-b)\operatorname{sn}^2[\delta\sqrt{b(a-c)}(t-t_0)|q]}, \quad (37)$$

where

$$q = \frac{a(b-c)}{b(a-c)}. \quad (38)$$

The period of the orbit T can be expressed in terms of the complete elliptic function of the first kind $K(q)$:

$$T = \frac{2}{\delta\sqrt{b(a-c)}}K(q) \quad (39)$$

and $R_3(t)$ can be written as

$$R_3(t) = \frac{bc}{b + (c-b)\operatorname{sn}^2[[2K(q)/T](t-t_0)|q]}, \quad (40)$$

Finally, the evolution equations for the other variables are

$$R_1(t) = R_3(t - T/3), \quad (41)$$

$$R_2(t) = R_3(t - 2T/3). \quad (42)$$

Summarizing, the behavior of the dynamical system in the case $\mu=0$ can be described as follows: after a transient time (or order 1) the three variables R_1 , R_2 , R_3 vary periodically in time on the plane $R_1 + R_2 + R_3 = 1$. When R_1 decreases, R_2 increases, etc. The period of the orbit depends only on the initial conditions through a constant of motion E . The explicit expression for the period, Eq. (39), shows that the period diverges logarithmically when E tends to zero, namely

$$T(E) = -\frac{3}{2\delta}\ln E \times (1 + O(E)), \quad (43)$$

and the amplitude of the oscillations $\Delta \equiv b - c$ depends also on the constant E . When E tends to 0 the amplitude approaches 1

$$\Delta = (1 - 2E^{1/2}) \times (1 + O(E)). \quad (44)$$

All these relations have been confirmed by a numerical integration of the Busse–Heikes equations. In Fig. 3 we plot the time evolution of the amplitudes in the case $\mu = 0$, $\delta = 1.3$. In this figure we can observe that, after an initial transient time, there is a periodic motion (characteristic of the Küppers–Lortz instability) well described by the previous analytical expressions.

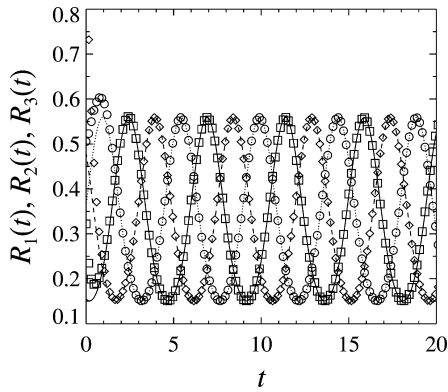


Fig. 3. Time evolution of amplitudes in the case $\delta = 1.3$, $\mu = 0$. After a transient time of order 1, the three variables R_1, R_2, R_3 vary periodically in time. The lines are the theoretical predictions that come from Eqs. (40), (41) and (42).

2.2. The case $\mu > 0$

Once we have understood the case $\mu = 0$, we now turn to $\mu > 0$. In this case, the function V is no longer a Lyapunov potential and we cannot reduce the motion to a Hamiltonian one on the surface of minima of V . However, since the main features of the Küppers–Lortz dynamics are already present in the case $\mu = 0$ one would like to perform some kind of perturbative analysis valid for small μ in order to characterize the Küppers–Lortz instability. We exploit these ideas in order to develop some heuristic arguments that will allow us to make some quantitative predictions about the evolution of the system.

According to Eq. (28), one can infer that $E(t)$ decreases with time in a characteristic time scale of order μ^{-1} . If μ is small, $E(t)$ decreases very slowly and we can extend the picture of the previous section by using an adiabatic approximation. We assume, then, that the evolution for $\mu > 0$ can be described by a Hamiltonian dynamics with an energy that slowly decreases with time. Hence, in reducing the energy, the system evolves by spiraling from a periodic orbit to another (similarly to a damped harmonic oscillator). Assuming this picture of a time-dependent energy $E(t)$, the main features of the case $\mu = 0$ can now be extended. This model has several predictions:

- After a transient time of order 1, the motion occurs near the plane $R_1 + R_2 + R_3 = 1$. This is checked in the simulations as we can see in Fig. 4 where we plot the time evolution of the three amplitudes as well as their sum, in the case $\delta = 1.3$, $\mu = 0.1$.
- The period of the orbits is now a function of time. Since the energy decreases towards zero, it follows from Eq. (43) that the period diverges with time. Moreover, it is possible to give an approximate expression for the time dependence of the period. By integration of Eq. (28), we obtain

$$E(t) = E(t_0)e^{-4\mu \int_{t_0}^t f(t') dt'} \approx E(t_0)e^{-4\mu(t-t_0)}, \tag{45}$$

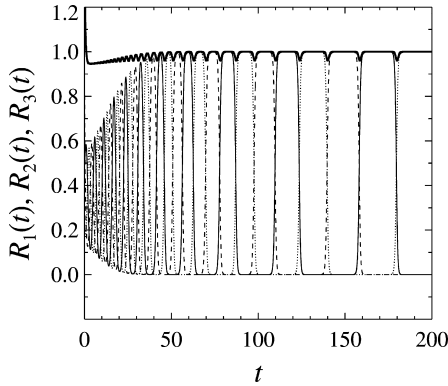


Fig. 4. Time evolution of amplitudes in the case $\delta = 1.3$, $\mu = 0.1$. The characteristic alternation time of the three variables R_1, R_2, R_3 increases with time. Note that the envelope of the amplitudes approaches one asymptotically, and that their sum, $R_1 + R_2 + R_3$ is approximately equal to 1.

where we have approximated $f(t)$ by its asymptotic value $f(t) = 1$. Once we have the time evolution of the energy, we can compute the time dependence of the period by using $T(t) = T(E(t))$ as given by (39). For late times, the energy is small and the asymptotic result (43) leads to

$$T(t) = T_0 + \frac{6\mu}{\delta} t. \tag{46}$$

This shows that the period increases linearly with time, in agreement with the results of [13] in which the residence period was shown to behave also linearly with time (although with a different prefactor). In order to check this relation, we have performed a numerical integration of Eqs. (2) and computed the period T , defined as the time it takes for a given amplitude to cross a reference level (taken arbitrarily as $R_j = 0.5$), as a function of time. The results for $\delta = \{1.3, 3\}$ and $\mu = \{0.1, 0.01\}$, plotted in Fig. 5, show that there is a perfect agreement between the theoretical expression and the numerical results.

- The amplitude of the oscillations, as given by the return points $\Delta(t) = b(t) - c(t)$ is now a function of time. Using expression (44) with an energy that decreases with time as in Eq. (45) we obtain that the amplitude of the oscillations increases with time (see Fig. 4), and that it approaches 1 in a time or order $t \sim \mu^{-1}$. More specifically, we have

$$1 - \Delta(t) = (1 - \Delta_0)e^{-2\mu t}. \tag{47}$$

In summary, for the case $\mu > 0$, the period of the orbits, which is a function of the energy, increases linearly with time and the amplitude of the oscillations approaches 1. We characterize in this way the increase of the period between successive alternation of the dominating modes (see Fig. 4), as an effect of the Hamiltonian dynamics with a slowly decreasing energy. This prediction of the Busse–Heikes model for the Küppers–Lortz instability is unphysical, since the experimental results do not show such an increase of the period. Busse and Heikes were fully aware of this problem

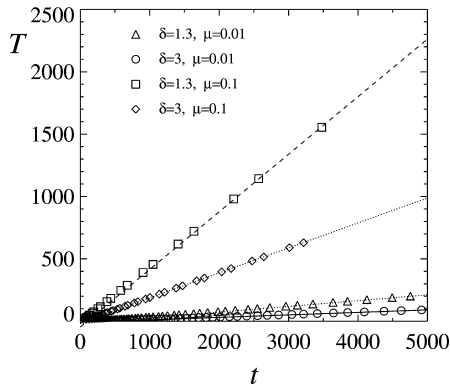


Fig. 5. Time evolution of the period, defined as the time it takes a given amplitude to cross the reference level $R_j = 0.5$ plotted versus time for several values of δ and μ . We also plot straight lines with slopes $6\mu/\delta$ as predicted by Eq. (46).

and suggested that noise terms (“small amplitude disturbances”), that are present at all times, prevent the amplitudes from decaying to arbitrary small levels and a motion which is essentially periodic but with a fluctuating period is established. In the next section we study the effect of noise in the dynamical equations.

3. Busse–Heikes model in the presence of noise

In order to account for the effect of the fluctuations, we modify the Busse–Heikes equations by the inclusion of noise terms

$$\begin{aligned}
 \dot{A}_1 &= A_1[1 - |A_1|^2 - (1 + \mu + \delta)|A_2|^2 - (1 + \mu - \delta)|A_3|^2] + \xi_1(t), \\
 \dot{A}_2 &= A_2[1 - |A_2|^2 - (1 + \mu + \delta)|A_3|^2 - (1 + \mu - \delta)|A_1|^2] + \xi_2(t), \\
 \dot{A}_3 &= A_3[1 - |A_3|^2 - (1 + \mu + \delta)|A_1|^2 - (1 + \mu - \delta)|A_2|^2] + \xi_3(t).
 \end{aligned}
 \tag{48}$$

We take the simplest case in which the $\xi_i(t)$ are, complex, white-noise processes [21] with correlations:

$$\langle \xi_i(t) \xi_j^*(t') \rangle = 2\epsilon \delta(t - t') \delta_{ij}.
 \tag{49}$$

As mentioned before, and in the case of parameter values lying inside the Küppers–Lortz instability region, noise prevents the system from spending an increasing amount of time near any of the (unstable) fixed points. The mechanism for this is that fluctuations are amplified when the trajectory comes close to one of the (unstable) fixed points of the dynamics and the trajectory is then repelled towards another fixed point [12]. Hence, a fluctuating, but periodic on average, trajectory is sustained by noise. Within the general picture developed in the previous section, the main role of noise for $\mu > 0$ is that of preventing $E(t)$ from decaying to zero. This can be understood

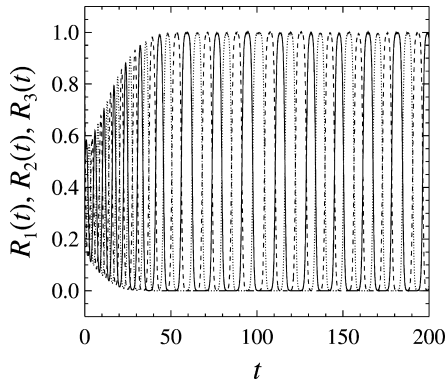


Fig. 6. Time evolution of amplitudes in the presence of noise for $\delta = 1.30$, $\mu = 0.1$, $\varepsilon = 10^{-7}$. In this case, the motion is such that the time interval between dominations of a single mode fluctuates around a mean value (compare with the equivalent deterministic case shown in Fig. 4).

in the following qualitative terms: when noise is absent, the dynamics brings the system to the surface of minima of V , where the dissipative terms act by decreasing the energy in a time scale of order μ^{-1} , see Eq. (45). The inclusion of noise has the effect of counteracting this energy decrease that occurs in the surface of minima of V . As a consequence, $E(t)$ no longer decays to zero but it stabilizes around a mean value $\langle E \rangle$. By stabilizing the orbit around that one corresponding to the mean value $\langle E \rangle$, fluctuations in the residual motion stabilize the mean period to a finite value. In order to check this picture, we have performed numerical simulations of Eqs. (48) for small noise amplitude ε , using a stochastic Runge–Kutta algorithm [19]. The numerical simulations (see Fig. 6), show indeed that the trajectories have a well-defined average period $\langle T \rangle$.

From a more quantitative point of view, and according to the previous picture, we can compute the mean period $\langle T \rangle$, which in the purely Hamiltonian case was a function of E (see Eq. (39)), by using the same function applied to the mean value of E , i.e., $\langle T \rangle = T(\langle E \rangle)$. This relation has been checked in the numerical simulations. In Fig. 7 we plot the mean period $\langle T \rangle$ versus the period calculated from the mean energy, $\langle E \rangle$, which has also been evaluated numerically. From this figure it appears that our qualitative argument of a trajectory stabilized around the Hamiltonian orbit, corresponding to the average energy, is well supported by the numerical simulations.

In order to proceed further, we consider the probability distribution for the amplitude variables, $P(A_1, A_2, A_3; t)$ which obeys a Fokker–Planck equation [22]. For a general dynamics of the type given by Eq. (8), it is possible to show [19] that the stationary probability distribution for the A_j variables is given by

$$P_{\text{st}}(A_1, A_2, A_3) = Z^{-1} \exp[-V(A_1, A_2, A_3)/\varepsilon],$$

$$Z = \int dA_1 dA_1^* dA_2 dA_2^* dA_3 dA_3^* e^{-V/\varepsilon}, \quad (50)$$

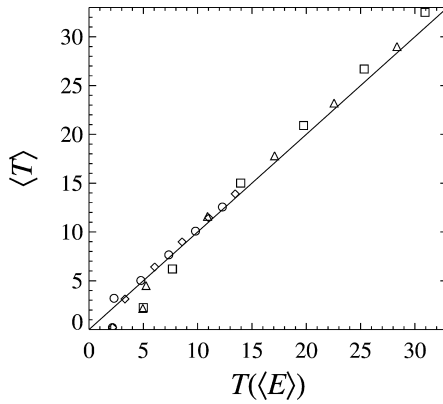


Fig. 7. Plot of the average period $\langle T \rangle$ plotted versus the theoretical value $T(\langle E \rangle)$ computed using the value of $\langle E \rangle$ obtained numerically. For each value of μ and δ (same symbols meaning than in Fig. 5) we use values of ε ranging from $\varepsilon = 10^{-2}$ to $\varepsilon = 10^{-7}$.

whenever two conditions are satisfied:

- (a) Orthogonality condition (12).
- (b) The residual dynamics [non-relaxational part of (8)] is divergence free

$$\sum_{j=1}^3 \frac{\partial v_j}{\partial A_j} = 0. \tag{51}$$

In our case of the Busse–Heikes equations the orthogonality condition is satisfied for $\mu = 0$, $\delta > 0$, and (51) is satisfied independently of μ and δ . For $\mu > 0$ this is no longer true but we expect that for small μ a relation similar to (50) would be valid if we replace V by a function Φ that differs from V in terms that vanish for vanishing μ . Using this probability distribution, one can compute the average value of the variable E as

$$\langle E \rangle = Z^{-1} \int dA_1 dA_1^* dA_2 dA_2^* dA_3 dA_3^* E \exp[-\Phi/\varepsilon]. \tag{52}$$

We take the crude approximation $\Phi = V$ and, after a change of variables to amplitude and phase, the mean value of the energy can then be computed as

$$\langle E \rangle = \frac{\int_0^\infty dR_1 \int_0^\infty dR_2 \int_0^\infty dR_3 E \exp[-V/\varepsilon]}{\int_0^\infty dR_1 \int_0^\infty dR_2 \int_0^\infty dR_3 \exp[-V/\varepsilon]}, \tag{53}$$

where V and E are given in terms of the variables R_1, R_2, R_3 in Eqs. (9) and (27), respectively. In the case $\mu = 0$ (for which the above expression is exact) we obtain the value $\langle E \rangle = \frac{1}{60}$, independent of ε , and $T = T(\langle E \rangle = \frac{1}{60}) \approx 6.4467/\delta$.

In the case $\mu > 0$, the above integral can be performed by means of a steepest descent calculation, valid in the limit $\varepsilon \rightarrow 0$, where it yields the asymptotic behavior $\langle E \rangle \rightarrow (\varepsilon/\mu)^2$. The mean period can now be computed, in this limit of small ε , using (43), with the result that the period, as a function of the system parameters δ, μ, ε ,

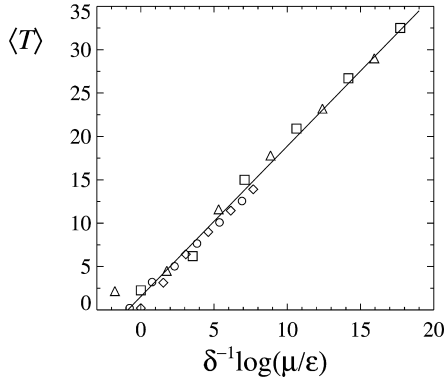


Fig. 8. Average period, $\langle T \rangle$, plotted as a function of $\delta^{-1} \log(\mu/\varepsilon)$ in order to check the predicted linear relation (54). The straight line is the best fit and has a slope of 1.73. Same symbols meanings than in Fig. 5 and values of ε ranging from $\varepsilon = 10^{-2}$ to $\varepsilon = 10^{-7}$.

behaves as

$$T(\varepsilon, \mu, \delta) \approx \frac{3}{\delta} \ln(\mu/\varepsilon), \tag{54}$$

a relation that is expected to hold in the limit of small ε and for small values of μ . The dependence with ε is the same than the one holding for the mean first passage time in the decay from an unstable state [19] and also follows from the general arguments of [12]. In Fig. 8 we show that there is indeed a linear relation between the period computed in the numerical simulations and $\delta^{-1} \ln(\mu/\varepsilon)$, as predicted by the above formula, although the exact prefactor 3 is not reproduced. We find it remarkable that, in view of the simplifications involved in our treatment, this linear relation holds for a large range of values for the parameters μ , δ and ε .

4. Spatial-dependent terms

Tu and Cross [9] have proposed an alternative explanation for the stabilization of the period without the necessity of the inclusion of the noise terms: they modify the Busse–Heikes equations by considering two-dimensional amplitude fields, $A_j(\mathbf{r}, t)$, and including terms accounting for the spatial variation of those fields

$$\begin{aligned} \partial_t A_1 &= \mathcal{L}_1 A_1 + A_1 [1 - |A_1|^2 - (1 + \mu + \delta)|A_2|^2 - (1 + \mu - \delta)|A_3|^2], \\ \partial_t A_2 &= \mathcal{L}_2 A_2 + A_2 [1 - |A_2|^2 - (1 + \mu + \delta)|A_3|^2 - (1 + \mu - \delta)|A_1|^2], \\ \partial_t A_3 &= \mathcal{L}_3 A_3 + A_3 [1 - |A_3|^2 - (1 + \mu + \delta)|A_1|^2 - (1 + \mu - \delta)|A_2|^2]. \end{aligned} \tag{55}$$

Here \mathcal{L}_j ($j = 1, 2, 3$) are linear differential operators. Two main classes of operators can be considered: isotropic and anisotropic. Whereas a multiple scale analysis of the convective instability usually leads to anisotropic terms, the isotropic terms are often justified for the sake of mathematical and numerical simplicity. There are also the

natural choice in problems of population dynamics [14]. The simplest isotropic terms are the Laplacian operators

$$\mathcal{L}_j^I = \nabla^2, \quad j = 1, 2, 3. \tag{56}$$

Two types of anisotropic terms have been proposed for similar fluid problems in the literature: (i) the Newell–Whitehead–Segel (NWS) terms [23,24] and (ii) the Gunaratne–Ouyang–Swinney (GOS) terms [25,26]. Without altering the essentials of the problem, both NWS and GOS terms can be further simplified leading to second-order directional derivatives along three directions with a relative orientation of 60° [9,27]:

$$\mathcal{L}_j^A = (\hat{\mathbf{e}}_j \cdot \nabla)^2, \quad j = 1, 2, 3, \tag{57}$$

which are the only anisotropic terms considered henceforth. These are more tractable numerically and will be used to compute the alternating period as explained below.

In this section we will compare the dynamical evolution corresponding to each one of the isotropic and anisotropic spatial dependent terms presented before, Eqs. (56) and (57), respectively.

Common to all of them is that, as in Section 2, we can recast system (55) into the form

$$\partial_t A_j(\mathbf{r}, t) = -\frac{\delta \overline{\mathcal{F}}_{\text{BH}}}{\delta A_j^*} + \delta v_j, \quad j = 1, 2, 3, \tag{58}$$

where $\overline{\mathcal{F}}_{\text{BH}}$ is a real functional of the fields given by

$$\begin{aligned} \overline{\mathcal{F}}_{\text{BH}}[A_1, A_2, A_3] = \int d\mathbf{r} \left[\sum_{j=1}^3 \left(\frac{1}{2} |\mathcal{L}_j^{1/2} A_j|^2 - |A_j|^2 + \frac{1}{2} |A_j|^4 \right) \right. \\ \left. + (1 + \mu)(|A_1|^2 |A_2|^2 + |A_2|^2 |A_3|^2 + |A_3|^2 |A_1|^2) \right] \end{aligned} \tag{59}$$

and the functions v_j are given by (10).

As in the zero-dimensional case of Sections 2 and 3, $\delta=0$ entails a relaxational gradient type dynamics and $\overline{\mathcal{F}}_{\text{BH}}$ acts as a Lyapunov functional that decreases monotonically with time. Since this potential is minimized by homogeneous solutions (because the spatial-dependent term gives always a positive contribution) the stationary solutions (and their stability) in the case $\delta = 0$ are the same as in the zero-dimensional case. Unfortunately, the orthogonality condition

$$\delta \sum_{j=1}^3 \int d\mathbf{r} \frac{\delta \overline{\mathcal{F}}_{\text{BH}}}{\delta A_j} v_j + \text{c.c.} = 0 \tag{60}$$

is not trivially satisfied in the case $\mu = 0$ for any of the spatial dependent terms mentioned before, and the dynamical equations cannot be reduced for $\mu = 0$ as in the zero-dimensional case.

In general, for $0 < \delta < \mu$, when the amplitudes grow from random initial conditions around $A_j = 0$, $j = 1, 2, 3$, we expect the formation of interfaces between the roll homogeneous states. Those interfaces move due to curvature and non-potential ($\delta > 0$) effects. Moreover, the fact of dealing with three fields allows the formation of vertices,

or points at which the three amplitudes take the same value. In the potential case, $\delta = 0$, the interface motion is such that a final state in which a unique roll solution fills the whole space is obtained (a process defined as “coarsening”). On the other hand, the non-potential dynamics induces the rotation of front lines around vertices giving rise to the formation of rotating spiral structures [28]. Similar structures have been observed in other three competing species systems, such as lattice voter models [29]. For small values of μ , the interfaces are wide (it can be shown that an interface varies over a length scale of order $1/\sqrt{\mu}$) and the density of vertices is low. For large μ the interfaces are sharp and the density of vertices increases. The exact shape of the spirals depends upon the spatial-derivative terms used. With the isotropic terms, Eq. (56), interface propagation follows the normal direction at each point so that closed domains have spherical shape and spiral structures are close to Archimedes’ spirals. On the other hand, for anisotropic spatial derivatives, Eq. (57), interface propagation no longer follows the normal direction and closed domains stretch or collapse along preferential directions so that they adopt an elliptic shape rather than a spherical one.

An important effect is that the rotation of interfaces around vertices, driven by non-potential effects, prevents the system from reaching a single roll solution filling the whole space, even outside the Küppers–Lortz instability region, i.e., for $\delta < \mu$ [30]. While this is true both for isotropic and anisotropic derivatives, the dynamical mechanism that prevents this coarsening is different for isotropic and anisotropic terms. For the isotropic terms, vertices of opposite sense of rotation annihilate initially with each other if located closer than a critical distance $d_c \sim \delta^{-1}$. After a transient time in which vertices are formed, they place each other outside the range of effective attraction of other vertices so that their number is essentially constant, thus preventing coarsening. For the anisotropic terms, two interfaces associated with the same vertex (and thus rotating in the same sense) may collide and generate continuously new vertices which, in turn, annihilate against each other again preventing coarsening outside the instability region. A consequence of interface motion is that a fixed point in space sees a change of the dominating amplitude. This alternation change is essentially periodic in time and presents a characteristic period which has nothing in common with the Küppers–Lortz instability mechanism in the bulk. Therefore, the period associated to this rotation is continuous at $\delta = \mu$, the instability point.

Before discussing what happens when this interface motion appears together with the instability in the bulk, we mention that for the isotropic terms it is possible to establish an analytical result concerning the front and spiral motion. In this case, using the fact that interfaces move in the normal direction to each point, it is possible to show that the rotation angular velocity of the interfaces around an isolated vertex scales, for small δ , as $\omega \sim \delta^2$ [30]. This predicts that, for the isotropic derivatives, the average period in a fixed point of space coming from the rotating spirals scales as $\langle T \rangle \sim \delta^{-2}$.

As mentioned above, the mechanism of front motion due to the non-potential effects coexists with the Küppers–Lortz bulk instability. We will show in the remaining of the section some results that follow, mainly, from a numerical integration of Eqs. (55) in two spatial dimensions. It appears from the numerical simulations that

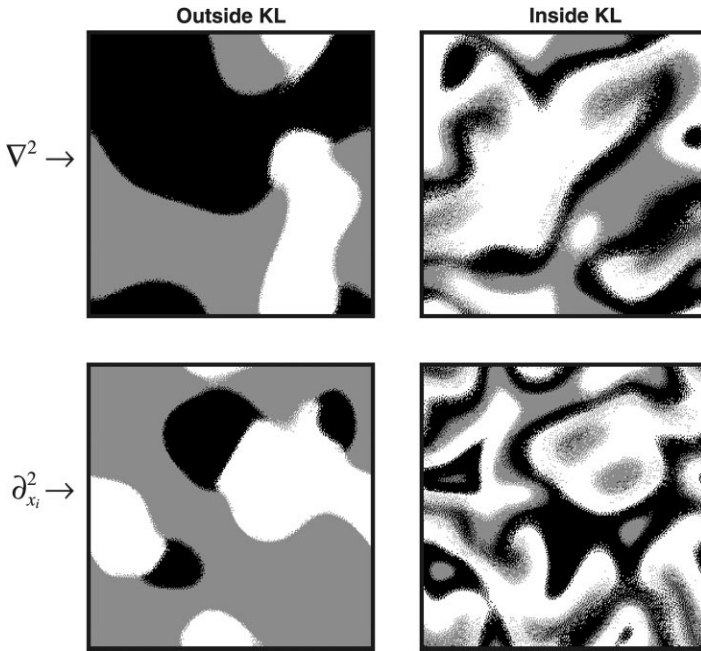


Fig. 9. Four snapshots at long times corresponding to a numerical simulation of the Busse–Heikes model [Eq. (55)] with isotropic ($\mathcal{L}_j^I = \nabla^2$) and anisotropic ($\mathcal{L}_j^A = (\hat{\mathbf{e}}_j \cdot \nabla)^2$) spatial derivatives. Parameter values are: $\mu = 0.1$ and $\delta = 0.05$ (1.3) outside (inside) the Küppers–Lortz instability region.

the behavior beyond the instability point (for $\delta > \mu$) depends strongly on the type of spatial derivatives used as well on the magnitude of the parameter μ . We discuss first each type of derivatives separately.

4.1. Isotropic derivatives

For μ small, the bulk instability is such that the intrinsic Küppers–Lortz period stabilizes to a statistically constant value. In a given point of space, we can see that the dominant amplitude changes due both to invasion from a rotating interface and a new amplitude growing inside the bulk. We give evidence of this combined mechanism in Fig. 9 where we have used the value $\mu=0.1$ and we present representative configurations inside and outside the instability region.

For higher values of μ , the Küppers–Lortz intrinsic period in the bulk is observed to increase with time. This is the same phenomenon that occurs in the zero-dimensional model without noise; see Section 2. Therefore at long times the Küppers–Lortz period is so large that we only see rotating interfaces around vertices, just like below the instability point. The two images of the upper row in Fig. 10 show domain configurations at long times for $\mu = 2.5$, below ($\delta = 2$) and beyond ($\delta = 3.5$) the Küppers–Lortz instability point in the case of the isotropic terms. Apart from the typical size of the

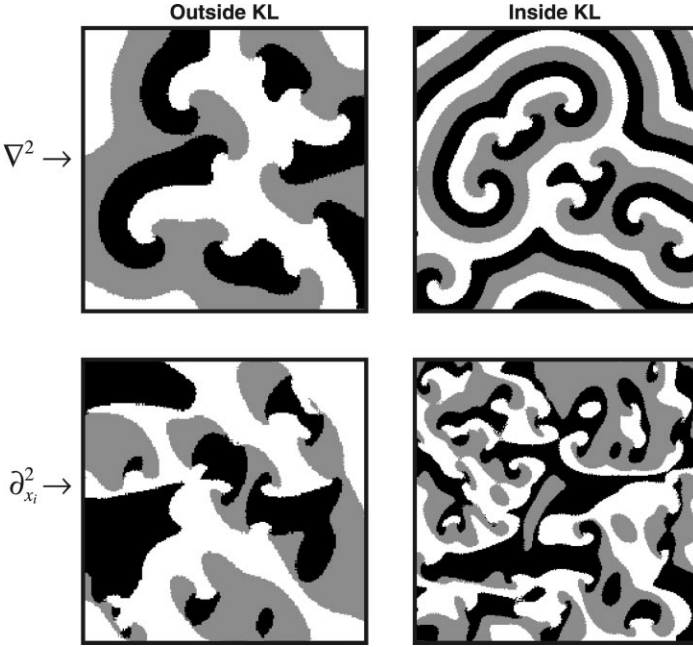


Fig. 10. Four snapshots at long times corresponding to a numerical simulation of the Busse–Heikes model [Eq. (55)] with isotropic ($\mathcal{L}_j^I = \nabla^2$) and anisotropic ($\mathcal{L}_j^A = (\hat{e}_j \cdot \nabla)^2$) spatial derivatives. Parameter values are: $\mu = 2.5$ and $\delta = 2$ (3.5) outside (inside) the Küppers–Lortz instability region.

domains, it appears that there is no qualitative difference between them. The period of alternating amplitudes is entirely dominated by front motion.

4.2. Anisotropic derivatives

Both for small and large μ , in the Küppers–Lortz regime, $\delta > \mu$, we observe, in addition to the front motion, domains of one phase emerging in the bulk of other domains; this is seen at all times, indicating that, at variance with the isotropic derivative case, the period associated with the Küppers–Lortz instability does not diverge with time. Evidence is given in Fig. 9 for $\mu = 0.1$ and Fig. 10 for $\mu = 2.5$, both figures showing results inside and outside the instability region.

For small μ , in summary, the morphology of domains inside and outside the instability region turns out to be similar with both kinds of spatial dependent terms, Fig. 9. The alternating period for $\delta > \mu$ is dominated by the Küppers–Lortz instability and is similar with isotropic and anisotropic spatial derivatives. This shows up in the fact that the period computed in a single point of space does not depend essentially of the type of derivatives used, as shown in Fig. 11a .

For large μ , on the other hand, the morphology is different for isotropic and anisotropic terms. For the isotropic ones, spiral rotation dominates the dynamics because of the very large period associated with the bulk instability. For the anisotropic terms, both

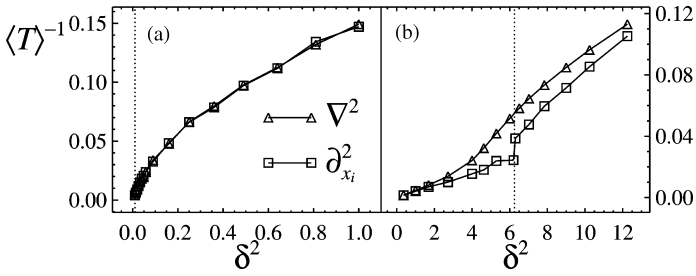


Fig. 11. Inverse of the alternating mean period as a function of δ^2 for the two-dimensional Busse–Heikes model with isotropic and anisotropic spatial-dependent terms. We have chosen the coordinates in order to emphasize the linear relation between the inverse of the period and δ^2 valid for small δ [26]. Each plot corresponds to a different value of the parameter μ . The Küppers–Lortz instability takes place at the right of the vertical dotted lines. (a) $\mu = 0.1$; (b) $\mu = 2.5$.

front motion and bulk instability are present. Finally in Fig. 11b (large μ) we show how the alternating period changes when going through the Küppers–Lortz instability. We first note that the period does not vanish in the stable regime ($\delta < \mu$). In this regime it is entirely due to front and spiral motion. For isotropic derivatives the period changes smoothly through the point $\delta = \mu$. This supports the fact that the period is still given by front motion for $\delta > \mu$. On the contrary, for anisotropic derivatives a jump in T is observed at $\delta = \mu$. In the Küppers–Lortz unstable regime and for anisotropic derivatives, T is determined by a combination of bulk instability and front motion.

5. Conclusions

We have analyzed the Busse–Heikes equations for Rayleigh–Bénard convection in a rotating fluid. For the situation of spatial-independent amplitudes, a case previously analyzed by May and Leonard, we find a Lyapunov potential that allows us, for $\mu=0$, to split the dynamics into a relaxational plus a residual part. Since the residual dynamics is Hamiltonian, we are able to give explicit relations for the time variation of the amplitudes and to compute the period of the orbits as a function of the energy, which, in turn, is a function of initial conditions. For $\mu > 0$ we extend the previous picture by using an adiabatic approximation in which the energy slowly decreases with time. This allows us to compute the variation of the alternation period between the three modes in the Küppers–Lortz instability regime. We next consider the effect of fluctuations and show how noise can stabilize the mean period to a finite value. By using the Lyapunov potential employed in the deterministic case, we can deduce an approximate expression that yields the period as a function of the system parameters, μ, δ as well as a function of the noise intensity ε . The conclusion is that the period increases logarithmically with decreasing noise intensity, a result that is well confirmed by numerical simulations

The two-dimensional version of this problem exhibits rather different dynamical behavior grossly dominated by vertices where three domain walls meet and which have no parallel in lower dimensional systems. The rotation of interfaces around vertices is

driven by non-potential effects and this inhibits coarsening for sufficiently large systems. We investigated the influence on the dynamics of the type of spatial-dependent terms. For small values of the parameter μ , the morphology of domains inside the Küppers–Lortz region turns out to be similar for both isotropic and anisotropic spatial derivatives. The alternating period is dominated by the Küppers–Lortz instability and is similar for both kinds of spatial-dependent terms. For large μ , on the contrary, the morphology of patterns as well as the alternating mean period are different for isotropic and anisotropic terms. While the intrinsic period of the instability diverges with time with isotropic derivatives, it saturates to a finite value in the anisotropic case.

Acknowledgements

We acknowledge financial support from DGESIC (Spain) projects numbers PB94-1167 and PB97-0141-C02-01.

References

- [1] G. Küppers, D. Lortz, *J. Fluid Mech.* 35 (1969) 609.
- [2] Y. Hu, R.E. Ecke, G. Ahlers, *Phys. Rev. E* 55 (1997) 6928.
- [3] Y. Hu, R.E. Ecke, G. Ahlers, *Phys. Rev. Lett.* 74 (1995) 5040.
- [4] Y. Ponty, T. Passot, P.L. Sulem, *Phys. Rev. Lett.* 79 (1997) 71.
- [5] H. Xi, J.D. Gunton, A. Markish, *Physica A* 204 (1994) 741.
- [6] M. Neufeld, R. Friedrich, *Phys. Rev. E* 51 (1995) 2033.
- [7] J. Millán-Rodríguez et al., *Chaos* 4 (1994) 369.
- [8] J. Millán-Rodríguez et al., *Phys. Rev. A* 46 (1992) 4729.
- [9] Y. Tu, M.C. Cross, *Phys. Rev. Lett.* 69 (1992) 2515.
- [10] M.C. Cross, D. Meiron, Y. Tu, *Chaos* 4 (1994) 607.
- [11] F.H. Busse, K.E. Heikes, *Science* 208 (1980) 173.
- [12] E. Stone, P. Holmes, *SIAM J. Appl. Math.* 50 (1990) 726.
- [13] R. May, W.J. Leonard, *SIAM J. Appl. Math.* 29 (1975) 243.
- [14] L. Fracheborug, P.L. Krapivsky, E. Ben-Naim, *Phys. Rev. E* 54 (1996) 6186.
- [15] A.M. Soward, *Physica D* 14 (1985) 227.
- [16] J. Guckenheimer, P. Holmes, *Nonlinear Oscillations, Dynamical Systems and Bifurcations of Vector Fields*, Springer, Berlin, 1983.
- [17] M. San Miguel, R. Montagne, A. Amengual, E. Hernández-García, in: E. Tirapegui, W. Zeller (Eds.), *Instabilities and Nonequilibrium Structures V*, Kluwer, Dordrecht, 1996.
- [18] R. Montagne, E. Hernández-García, M. San Miguel, *Physica D* 96 (1996) 47.
- [19] M. San Miguel, R. Toral, in: E. Tirapegui, W. Zeller (Eds.), *Instabilities and Nonequilibrium Structures, VI*, Kluwer, Dordrecht, 1999.
- [20] M. Abramowitz, I. Stegun (Eds.), *Handbook of Mathematical Functions*, Dover, New York, 1970.
- [21] N.G. van Kampen, *Stochastic Processes in Physics and Chemistry*, North-Holland, Amsterdam, 1981.
- [22] H. Risken, *The Fokker–Planck Equation*, Springer, Berlin, 1984.
- [23] A.C. Newell, J.A. Whitehead, *J. Fluid Mech.* 38 (1969) 279.
- [24] L.A. Segel, *J. Fluid Mech.* 38 (1969) 279.
- [25] G.H. Gunaratne, Q. Ouyang, H.L. Swinney, *Phys. Rev. E* 50 (1994) 2802.
- [26] R. Graham, *Phys. Rev. Lett.* 76 (1996) 2185.
- [27] B. Echebarria, H. Riecke, preprint ptt-sol/9912002.
- [28] R. Gallego, M. San Miguel, R. Toral, *Comput. Phys. Commun.* 121–122 (1999) 324.
- [29] G. Szabó, M.A. Santos, J.F.F. Mendes, preprint, cond-mat/9907333.
- [30] R. Gallego, R. Toral, M. San Miguel, in preparation.